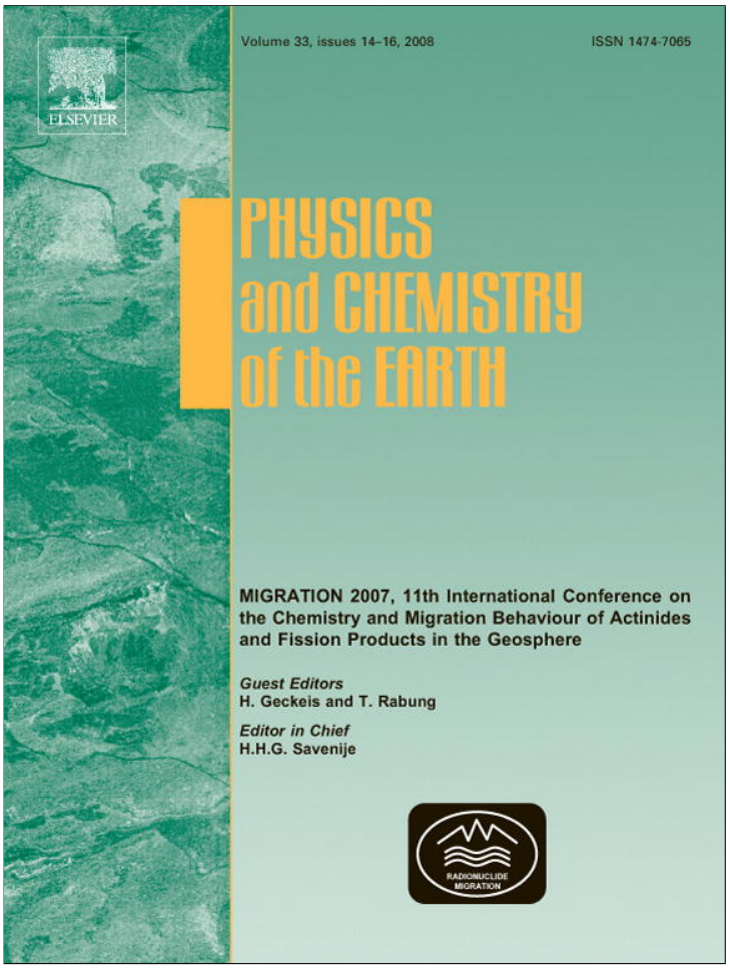

Physics and Chemistry of the Earth 33 (2008) 1042–1049

Contents lists available at ScienceDirect

Physics and Chemistry of the Earth

journal homepage: www.elsevier.com/locate/pce

Radionuclide transport in fractured granite interface zones

Q.H. Hu [a,b,*], A. Möri [c]

[a] College of Water Sciences, Beijing Normal University, Xinjiekouwai Street 19, Beijing 100875, PR China
[b] Atmospheric, Earth, and Energy Division, Lawrence Livermore National Laboratory, 7000 East Avenue, Livermore, CA 94550, USA
[c] Institute of Geological Sciences, University of Bern, Switzerland

ARTICLE INFO

Article history:
Available online 7 June 2008

Keywords:
Radionuclide
Diffusion
Transport
Granite
Grimsel Test Site

ABSTRACT

In situ radionuclide migration experiments, followed by excavation and sample characterization, were conducted in a water-conducting shear zone at the Grimsel Test Site (GTS) in Switzerland to study migration paths of radionuclides in fractured granite. In this work, a micro-scale mapping technique was applied by interfacing laser ablation sampling with inductively coupled plasma-mass spectrometry (LA-ICP-MS) to detect the small scale (micron-range) distribution of actinides in the interface zones between fractures and the granitic rock matrix. Long-lived ^{234}U, ^{235}U, and ^{237}Np were detected in flow channels, as well as in the diffusion accessible rock matrix, using the sensitive, feature-based mapping of the LA-ICP-MS technique. The retarded actinides are mainly located at the fracture walls and in the fine grained fracture filling material as well as within the immediately adjacent wallrock.

The water-conducting fracture studied in this work is bounded on one side by mylonite and the other by granitic matrix regions. Actinides studied in this work did not penetrate into the mylonite side as much as into the granite matrix, most likely due to the lower porosity, the enhanced sorption capacity and the disturbed diffusion paths of the mylonite region itself. Overall, the maximum penetration depth detected with this technique for ^{237}Np and uranium isotopes over the field experimental time scale of about 60 days was about 10 mm in the granitic matrix, illustrating the importance of matrix diffusion in retarding radionuclide transport from the advective fractures. Laboratory tests and numerical modelling of radionuclide diffusion into granitic matrix was conducted to complement and help interpret the field results.

1. Introduction

Matrix diffusion is recognized as an important process in retarding radionuclide transport in fractured rocks. In the last three decades, there has been an increased appreciation of the importance of matrix diffusion in the transport of solutes and implications in contaminant remediation and waste management (e.g., Neretnieks, 1980; Grisak and Pickens, 1980; Abelin et al., 1991; Maloszewski and Zuber, 1993; Novakowski and Lapcevic, 1994; Hadermann and Heer, 1996; Meigs and Beauheim, 2001; Hu et al., 2001; Salve et al., 2004; Zhou et al., 2006; Möri et al., 2006; Dai et al., 2007). However, there have been few long-term field-scale experiments to realistically evaluate matrix diffusion of radionuclides in fractured rock with minimal disturbance to the *in situ* condition. Changes to the pore spaces near the fractures (mineralogical alteration and mechanical deformation), and the presence of a complex system of connected pore types within the unaltered matrix, will influence the radionuclide distribution and residence time in the rock matrix (Möri et al., 2003; Sardini et al., 2006). This work is part of an ongoing long-term diffusion (LTD) project conducted at the Grimsel Test Site (GTS) to further study the long-term *in situ* diffusion of radionuclides in fractured rocks.

The GTS is an underground rock laboratory that has been operated since 1984 by the Swiss National Co-operative for the Disposal of Radioactive Waste (NAGRA). The site is licensed for *in situ* experiments with radionuclides in water-conducting features and in matrix rocks, and thus has been used over the past two decades for various transport studies with radionuclides (Alexander et al., 1992; Hadermann and Heer, 1996; Eikenberg et al., 1998; Frieg et al., 1998; Smith et al., 2001). Migration experiments with dyes, homologues and various radionuclides including actinides had been conducted since 1988 in a well defined shear zone located in the granodioritic host rock at the GTS. In 1993 three *in situ* tracer injections with sorbing ^{137}Cs were carried out in a saturated 1.7 m long dipole flow field within the test shear zone followed three years later in 1996 by a number of *in situ* tracer tests including

* Corresponding author. Address: College of Water Sciences, Beijing Normal University, Xinjiekouwai Street 19, Beijing 100875, PR China. Tel.: +86 10 58802738; fax: +86 10 62209289.
E-mail address: huqinhong@yahoo.com (Q.H. Hu).

1474-7065/$ - see front matter © 2008 Elsevier Ltd. All rights reserved.
doi:10.1016/j.pce.2008.05.015

long-lived ^{234}U, ^{235}U and ^{237}Np. Injection and extraction flow rates were constant at 8.1 ± 0.2 and 158 ± 1 mL/min, respectively (Eikenberg et al., 1998). Two months after these injections, the *in situ* flow field was stabilised by injecting a fluoresceine-doped epoxy resin and then excavated by overcoring with two 300 mm boreholes parallel to the shear zone. The overcores were sliced and radionuclide retardation sites along the flow paths were detected by β/γ-autoradiography (Möri et al., 2006).

In this work, selected drillcore samples were used to investigate the effects of structural/mineralogical features on the diffusion of radionuclides (long-lived ^{234}U, ^{235}U, and ^{237}Np) from the flow channels into the adjacent rock matrix. Using a sensitive, multi-elemental, micro-scale mapping technique (Hu et al., 2004) that interfaces laser ablation sampling with inductively coupled plasma-mass spectrometry (LA-ICP-MS), we determined the distribution of these actinides along profiles perpendicular to the flow paths. Laboratory tests and numerical modelling of radionuclide diffusion into granitic matrix was conducted to complement and help interpret the field results by determining diffusion rates.

2. Materials and methods

2.1. Description of field samples

The test shear zone consists of an array of cleavage parallel fracture planes which are separated by weakly deformed granite matrix. The investigated rock samples contain three principal rock domains that are present in a water-conducting feature at the GTS (for details see Bossart and Mazurek, 1991; Möri et al., 2006): granite matrix, mylonite, and fracture filling material (cohesionless fault breccia and/or fault gauge). These rock types are the result of the complex deformation history of the variscian Central Aare granite and Grimsel granodiorite. The regional greenschist metamorphism leads to the evolution of a penetrative foliation followed by increased ductile deformation during the alpine orogeny forming the still present mylonitic shear zones. Mylonitic deformation leads to re-crystallisation with grain-size reduction and preferred grain orientation. Compared to the surrounding rock matrix, the mineralogical composition of the mylonite is reduced in quartz and K-feldspar and slightly increased by albite and biotite content. Later deformation steps at lower temperature lead to brittle deformation which in general followed the mylonitic shear bands. This deformation had mechanical effects on the rock. The rock fabric was destroyed and with increasing deformation the rocks along the fracture planes were grind and thus formed breccia and fault gouge.

The different deformation styles also influence the formation of flow paths and transport parameters such as porosity and hydraulic conductivity. Mylonitisation lead to a reduction in porosity and no additional flow path were formed in this deformation. Undisturbed mylonite in the test shear zone has porosities below 0.5% compared to the granitic matrix which reveals porosities around 1%.[1] In contrast, the brittle deformation leads to discrete openings and enhanced porosities in the fracture filling material. Fault gouge shows high porosities of 10–30% and, due to its friable nature, it facilitates the formation of open flow channels which significantly increase the hydraulic conductivity.

2.2. LA-ICP-MS analyses

Laser ablation is the process by which an intense burst of energy delivered by short laser pulses is used to vaporize a minute (nanogram-range) sample from a specific location. The chemical composition of the vaporized sample is then analyzed by an inductively coupled plasma-mass spectrometer. Since 1985, laser ablation coupled with ICP-MS has evolved as a powerful analytical tool for *solid* sampling and analysis (e.g., Russo et al., 2000, 2002; Sylvester, 2005). LA-ICP-MS can simultaneously detect a large number of chemical elements at low detection limits, typically in the range of nanograms to low micrograms per gram.

In this study, the CETAC LSX-200 laser ablation system was used (CETAC Technologies, Omaha, NE), interfaced with the X-Series ICP-MS (Thermo Electron Corporation, West Palm Beach, FL) to characterize the distribution of radionuclides in the granitic samples. During data acquisition, signal intensities (counts per second, cps) were recorded for a number of elements, including the radionuclides of interest (^{234}U, ^{235}U, and ^{237}Np) and other elements intrinsic to the rock (e.g., ^{29}Si, ^{85}Rb, ^{137}Ba, and ^{232}Th). After laser firing, there was about a 10-s pause, during which the signal intensity measured was used to determine the instrument background for each element, before the ablated sample material was transported to the ICP-MS detector for elemental detection. When the sample reached the detector, there was a sharp rise in signal intensity, followed by a gradual decrease in intensity to near-background levels within several minutes after laser firing. The integrated signal intensity data are obtained, after subtracting the background, by adding all signals. Differences in the integrated signal intensity of the elements reflect their differences in concentration in the sample matrix (Hu et al., 2004). The radionuclide distribution in the field samples is represented by the uranium ratios ($^{238}U/^{234}U$, $^{238}U/^{235}U$ and $^{234}U/^{235}U$) and by the signal response for ^{237}Np (cps normalized by numbers of laser pulses for comparison).

The spot size dictates the spatial resolution during the surface mapping with the LA-ICP-MS method and the number of laser pulses fired at each sampling spot determines the amount sampled as well as the corresponding sampling depth (each laser pulse digs a crater at about 0.8 μm deep). Spot size and number of laser pulses had to be optimized to meet the sampling objectives of this study. For the coarse-grained granite, a relatively large spot size of 0.3 mm was used to mitigate the difference in porosity and grain-size of rock matrix to achieve representative sampling. Coupled with 20 laser pulses at each sampling spot, a moderate amount of rock was ablated for the detection of trace amounts of the radionuclides present in the samples.

The concentration of an analyte can be semi-quantitatively assessed by measuring a reference element with a known concentration in both the unknown and reference samples (e.g., the internal standard). ^{29}Si as one of the major element constituents of a granite was chosen as the reference element. The normalized ratio of analyte to internal standard for the LA-ICP-MS analysis of both the sample and reference standards (NIST SRM 616, 614, 612, and 610) was then used to calculate the analyte concentration. As a semi-quantitative survey tool, the technique provides useful insights into spatial distribution of compositional heterogeneities that would be otherwise overlooked during conventional bulk analytical measurements.

2.3. Laboratory diffusion test

Diffusion tests under saturated conditions were conducted to investigate tracer diffusion into cylindrical (10 mm wide and 10 mm high) GTS granite samples, which had been fully saturated (with the help of vacuum pulling) with a typical groundwater of dilute Na–K–HCO_3 constituents. The saturated sample was placed on a Teflon mesh inside a plastics container (Fig. 1). Only the bottom part of the sample was in contact with the tracer solution in the container in order to minimize hydraulic head difference. To maintain nearly constant tracer concentration in the reservoir a large

[1] Porosity values were determined with the mercury porosimetry method on lab samples.

Fig. 1. Photo showing the saturation diffusion apparatus. The white Teflon was used to prevent the sample from moving during the stirring.

volume was chosen compared to the pore volume of the sample (abut 800 mL compared to <0.01 mL pore volume of the sample). The tracer reservoir was stirred constantly with a magnetic stirrer. The lidded container was placed inside an incubator with a controlled temperature of 23 °C. After about 20 h of contact time, the diffusion was stopped and the sample was placed inside a −80 °C freezer, followed by freezer-drying and dry storing for LA-ICP-MS analysis.

Non-radioactive species, chemical homologues and radionuclides were employed in investigating the diffusion process of radionuclides in granitic rock samples. The radionuclides that were used are ^{237}Np and ^{235}U. Homologues were chosen based on their chemical similarity to radionuclides of interest. Non-radioactive caesium was substituted for radioactive ^{137}Cs. Perrhenate (ReO_4^-) served as a conservative tracer and nickel as a homologue for cobalt (Eikenberg et al., 1998).

Different from the commonly used through-diffusion approach in which the tracer concentrations in the source and/or sink reservoirs are measured, the tracer concentration distribution in the rock sample is directly mapped on the rock sample. Therefore, this technique allows short experimental duration (hours versus days for the through-diffusion approach) and works for the strongly-sorbing tracers that would not break through in the through-diffusion approach within reasonable time scales.

3. Results and discussion

3.1. Detection of radionuclides in field samples

To map the radionuclide distribution in and around an advective flow path, a slab (ID: A6-5) with several visible advective flow paths was used. A quarter of the slab containing the major fracture is shown in a photo in Fig. 2A. Using γ-spectrometry, this slab was measured to a bulk radioactivity of 7.5×10^3 Bq for ^{137}Cs. The other radionuclides of interest were below detection limit for bulk activity measurements with γ-spectrometry (<1.28×10^2 Bq for ^{60}Co, <2.37×10^2 Bq for ^{235}U and 2.68×10^2 Bq for ^{237}Np). The spatial distribution of radionuclides along the flow paths as well as within the adjacent matrix was detected by means of a new β/γ-autoradiography scanner (Möri et al., 2006). The application of β/γ-autoradiography allowed to investigate a large number of rock samples and to study the activity distribution in and around the flow paths. First evaluations on these autoradiographs revealed that activity was mainly concentrated on matrix rock portions adjacent to the flow paths. Even though the resolution of the autoradiographs is limited by the natural scatter of the gamma radiation, the autoradiographs delivered first indications on diffusion paths along grain boundary pores.

With this spatial information, square-shaped sub-samples (32 mm each side, suitable for being placed inside the laser ablation chamber for analyses) were cut such that they focus on the regions around the advective flow path (Fig. 2B). In this particular part of the shear zone, the flow path is bounded on one side by a biotite rich mylonite with a thickness varying from 7 to 11 mm, and on the other side by almost undisturbed granitic rock matrix (Fig. 2D).

Table 1 lists the amount of radionuclides injected into the test shear zone 2 months before immobilization by *in situ* resin injection and excavation. The majority of these radionuclides are relatively short-lived, with high specific activity suitable for radiometric analyses (Eikenberg et al., 1998; Möri et al., 2006). At the opposite, the long-lived actinides applied are suitable for mass spectrometric analyses to detect their presence in the excavated rock samples.

LA-ICP-MS analyses were performed to monitor the signal response of various elements, including those intrinsic to the rock (e.g., ^{29}Si, ^{44}Ca, ^{85}Rb, ^{137}Ba, and ^{232}Th) as well as the tracers shown in Table 1. The low concentrations of the fission products ^{60}Co and ^{137}Cs were effectively masked by isobaric interferences with the Ni and Ba content in the rock; ^{60}Ni has a natural abundance of 26.2% and ^{137}Ba 11.3% natural abundance.[2] Similarly, the atomic masses 113 and 152 for injected radionuclides ^{113}Sn and ^{152}Eu were monitored, but the isobaric interference of ^{113}Cd and ^{152}Sm prevent the mass spectrometric detection of these radionuclides due to low initial activity, low recovery, and decay of ^{113}Sn. Finally, ^{75}Se was found to pass the flow field almost unretarded and could not be detected in the rock (Table 1).

Although similar masking issues may be encountered with actinide species, there are less mass interferences at high mass numbers because of the smaller number of naturally-occurring isotopes in this mass range. Because of the high amount of actinides injected into the shear zone (Table 1), their presence in the rock samples is unambiguously detected, as shown in Fig. 2. Long-lived ^{234}U, ^{235}U, and ^{237}Np were detected on flow channels, as well as in the adjacent rock matrix, using the sensitive, feature-based and micro-scale mapping of the LA-ICP-MS technique. Increased activity above natural background was observed both in the water-conducting fracture and in the adjacent rock matrix.

3.2. Structural and mineralogical controls on radionuclide transport

^{237}Np signal response and ^{235}U/^{238}U ratios were determined along several profile lines crosscutting the flow path with two different kinds of wall rock: mylonite and granite. Figs. 3 and 4 show the sampling spots along two profile lines in sub-samples A2 and A4. Photos taken during the laser ablation for each sampling spot, along with the distance between the spots, are shown to the left of the figures. The type of spots sampled is indicated (matrix: granite; wall: fracture wall; fracture: advective flow path impregnated by the resin which may contain fracture infill), as well as the corre-

[2] Barium and nickel are expected to have concentrations in granite as high as several hundred milligrams per kilogram; for example, the reported barium concentration in the granite of Stripa mine of Sweden is 545 ± 60 mg/kg (Nordstrom et al., 1989). This is at least two orders of magnitude higher than the expected concentrations of ^{60}Co and ^{137}Cs, even we assume all the measured radioactivity of these radionuclides in the whole slab is concentrated in a thin layer of 1 mm thickness with a length of 100 mm.

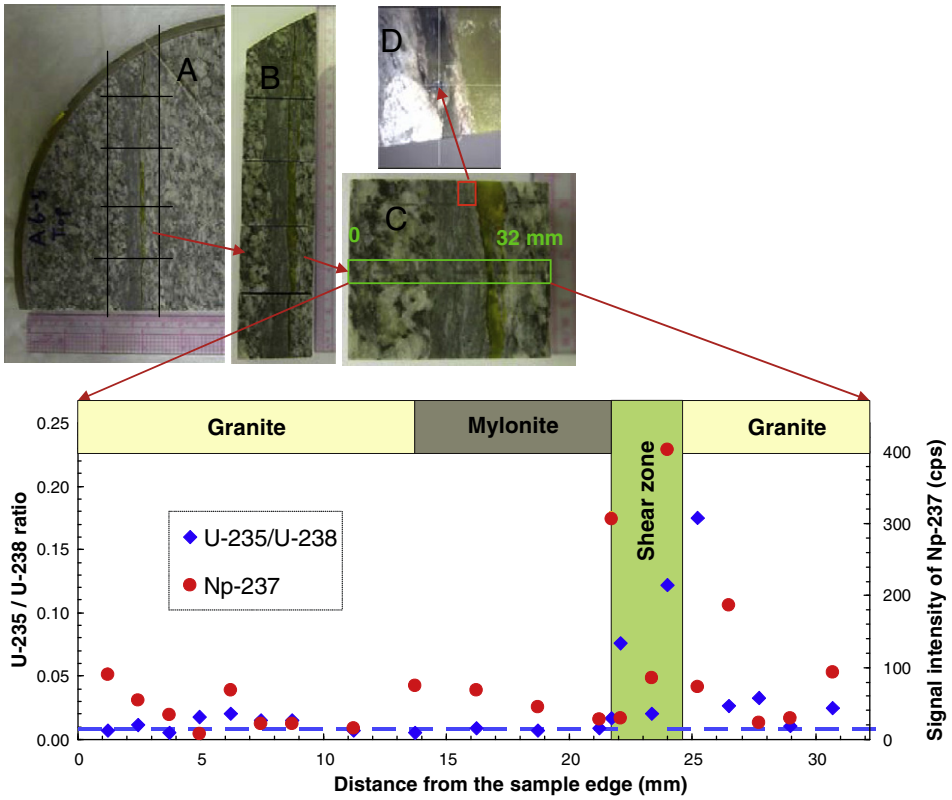

Fig. 2. Sample processing steps (A–D) with profile trace for $^{235}U/^{238}U$ ratio and ^{237}Np signal (normalized cps per laser pulse) measurements across the flow path. The dashed line represents the natural $^{235}U/^{238}U$ ratio of 0.0072.

Table 1
Compilation of relevant radionuclides used in dipole test at the GTS

Radionuclide	Half-life (year)[a]	Injected amount		Mass recovery (%)
		Radioactivity (Bq)[b]	Mass (nmol)	
^{60}Co	5.27	$(2.03 \pm 0.05) \times 10^6$	0.808	20
^{75}Se	0.328	$(1.08 \pm 0.08) \times 10^7$	0.267	95
^{113}Sn	0.315	$(1.93 \pm 0.10) \times 10^6$	0.0459	~5
^{137}Cs[c]	30.2	1.88×10^7	42.7	>70
^{152}Eu	13.5	$(2.96 \pm 0.10) \times 10^5$	0.302	~20
^{233}Pa[d]	0.0739	$(5.80 \pm 0.40) \times 10^5$	0.00324	~25
^{234}U	246,000	$(5.74 \pm 0.37) \times 10^5$	10,677	~50
^{235}U	704,000,000	$(1.54 \pm 0.10) \times 10^4$	819,810	~50
^{237}Np	2,144,000	$(5.80 \pm 0.60) \times 10^5$	94,033	~25%

[a] From Lide (2000).
[b] Eikenberg et al. (1998).
[c] Three tracer tests were carried out in 1993, injecting ^{137}Cs each time between 6.0×10^6 and 6.5×10^6 Bq (Möri et al., 2006).
[d] Short-lived progeny ^{233}Pa in secular equilibrium with its long-lived parent ^{237}Np in the injected solution.

sponding radionuclide signals. Included are also the uranium ratios in nature and the instrumental background for ^{237}Np, as well as the uranium ratios from the tracer cocktail. Highest activities were found within the flow path either in the fracture filling material or at the surface of the wall rock. Uranium and neptunium were also detected in the adjacent granitic rock matrix (Fig. 2C, right side of the shear zone) to a depth of about 7 mm.

Low concentrations of ^{237}Np were observed within the mylonite region as well as behind the mylonite in the granitic matrix (Fig. 2C, left side). At the opposite side of the flow path, ^{237}Np concentrations in the rock matrix are much higher in the first 5 mm. However, the distribution in the matrix is irregular, indicating grain boundary diffusion in coarsely-grained granite with mineral sizes of several millimetres, which are larger than the sampling spot size for the LA-ICP-MS (0.3 mm). Similar observations were made with the β/γ-autoradiographs, giving clear evidence of grain-boundary-controlled radionuclide retardation sites in the rock matrix (Möri et al., 2006).

The distribution of ^{235}U and ^{234}U follows the general trend of ^{237}Np, with almost no detectable activity within and behind the mylonite but increased activity in the granitic rock matrix on the other side of the flow path (Figs. 2-4). Due to the very low instrumental background, which was measured to be about 0.5 normalized cps (normalized by the number of laser shots fired for sampling), and the lack of naturally-occurring ^{237}Np in the sample, LA-ICP-MS can detect very small amounts (about 10^{-4} mg/kg) of injected ^{237}Np remaining in the granite. The relatively small injected mass of ^{234}U leads to a smaller signal response as indicated from the $^{234}U/^{235}U$ ratio, with a ratio of 0.013 in the injected solution and a natural ratio of 0.00764 (Fig. 3). On the other hand, the signal response for $^{238}U/^{235}U$ is about a factor of 200 for a sampling spot (No. 3 in sub-sample A4) with a ratio of 0.658, indicating a high presence of ^{235}U in this sample location (Fig. 4).

The mylonite appears to hinder radionuclide transport from the flow path into the adjacent formation. This is especially clear from the asymmetrical distribution of ^{237}Np around the flow path, which has a higher signal response for the LA-ICP-MS measurements than the uranium isotopes (Figs. 2-4). Note that a relatively high signal detected for a radionuclide at a particular location might be a combination of diffusive transport and high sorption. While sampling spot 2 in sub-sample A2 (Fig. 3) at the fracture wall indicates 306 cps for ^{237}Np, the ^{237}Np signal 500 μm away within the mylonite decreases to 27.4 cps. Furthermore, the sampling spot 2 in sub-sample A4 (Fig. 4) inside the mylonite shows a ^{237}Np signal of 71.8 cps which is clearly lower than sampling

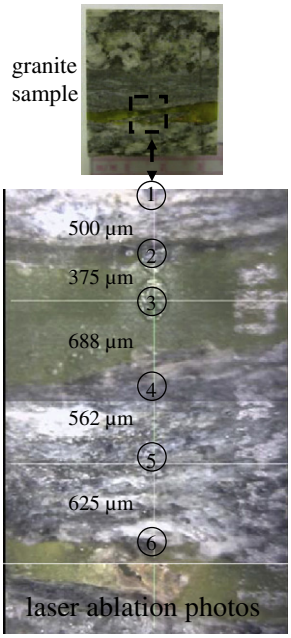

Sampling spot	$^{238}U/^{235}U$	$^{234}U/^{235}U$	^{237}Np (cps)
1 (mylonite)	109	0.0116	27.4
2 (wall / fracture)	61.1	0.0096	306
3 (fracture)	13.1	0.0157	29.4
4 (matrix)	132	0.0082	51.3
5 (matrix)	49.4	0.0131	85.9
6 (matrix / fracture)	8.23	0.0116	402
Natural	138	0.00764	~0.5
Tracer	< 1	0.0130	

Fig. 3. LA-ICP-MS sampling spots (circled areas) on sub-sample A2 with uranium ratios and neptunium counting rates (normalized cps per laser pulse). This sub-sample (32 mm each side) has two water-conducting fractures (widths about 1 and 0.4 mm).

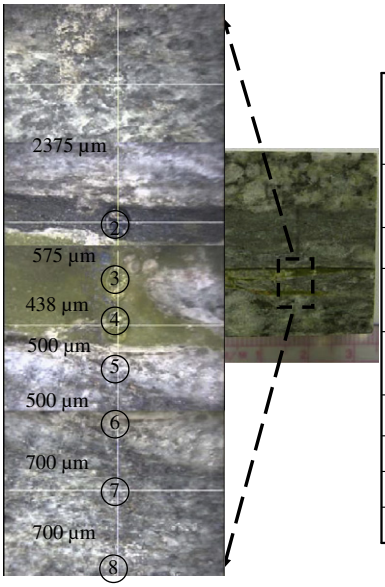

Sampling spot	$^{238}U/^{235}U$	$^{234}U/^{235}U$	^{237}Np (cps)
1 (mylonite)	152	0.0221	38.6
2 (wall)	24.0	0.0077	71.8
3 (fracture)	0.658	0.0146	474
4 (fracture)	4.28	0.0127	261
5 (matrix)	94.0	0.0143	119
6 (matrix)	113	0.0060	46
7 (matrix)	130	0.0093	28.8
8 (matrix)	52.0	0.0106	15.8

Fig. 4. LA-ICP-MS sampling spot areas on sub-sample A4 with uranium ratios and neptunium counting rates: width of flow path: 1 mm.

spots 3 and 4 located within the fracture filling material (261 and 474 cps, respectively). Also sampling spot 5 in the granitic matrix on the other side of the shear zone shows increased activity compared to the mylonite (119 cps).

3.3. Laboratory diffusion measurements

Laboratory tests on saturated undeformed granite samples were conducted to independently obtain the apparent diffusivity of Co, Cs, U, and Np used in the field dipole test. Fig. 5a presents the diffusion profiles which were measured with LA-ICP-MS for these tracers, with nickel serving as a homologue for cobalt and rhenium (ReO_4^-) behaving as a non-sorbing species. The background line for each tracer is also presented in Fig. 5a, with the background signals coming from the tracer's intrinsic presence in the granite, isotopic- and polyatomic-mass interferences, or from the instrumental background. Compared with the background levels, the input signal measured at the bottom of the granite sample varies from about two orders of magnitude larger for caesium (with its relatively high concentration in granite – about 1 mg/kg when measured from a clean sample) to more than four orders for neptunium, which has very low interference. Diffusion of non-retarded ReO_4^- has crossed the 10-mm sample length within the diffusion duration of nearly 20 h. All other tracers have diffusion profiles showing retardation from their interactions with the granite minerals.

A numerical simulator called HYDRUS-1D was used to fit the obtained diffusion profiles. The software package can simulate

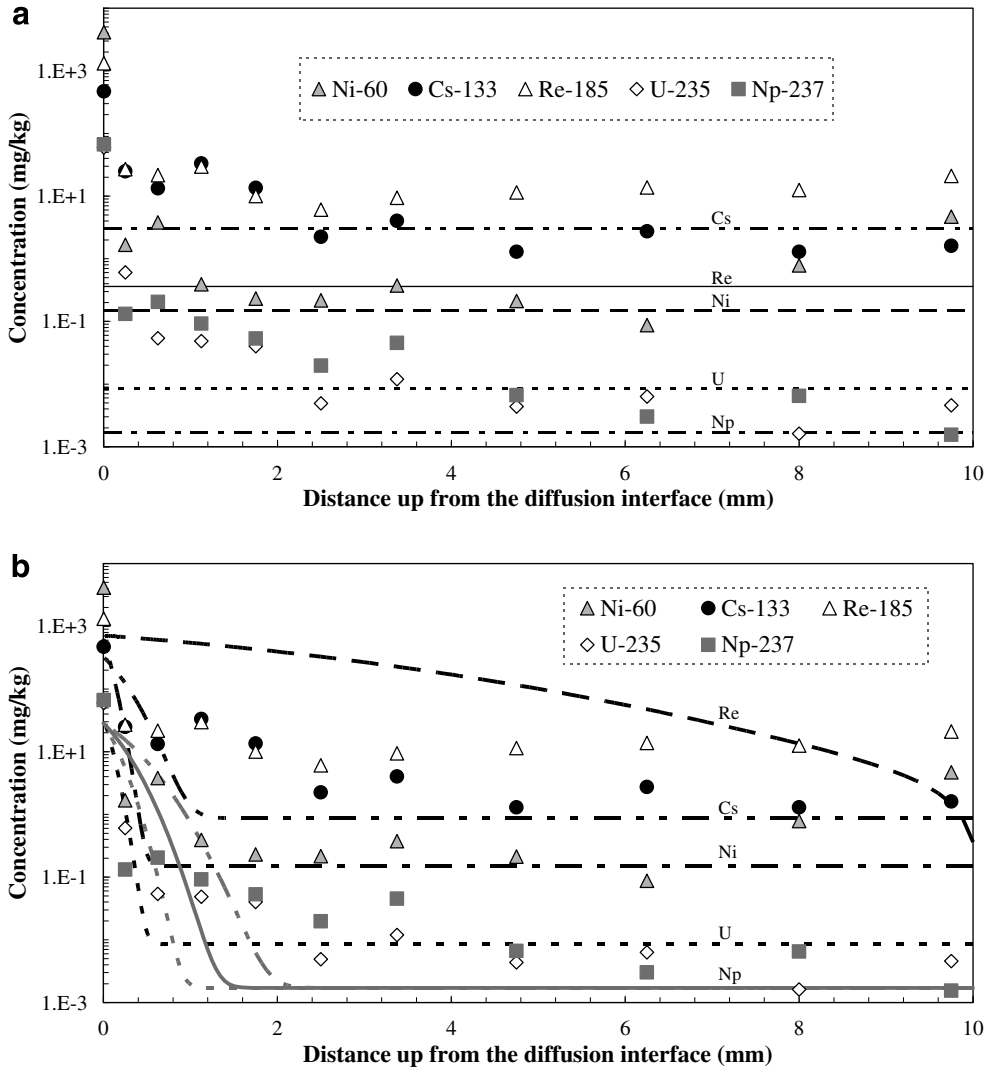

Fig. 5. (a) Experimental data of tracer diffusion profiles in saturated granite. Dashed lines are the averaged background levels of tracers. The averaged source concentrations measured at the bottom (diffusion interface is zero) for tracers are 630, 329, 715, 36.0, 28.4 mg/kg for Ni, Cs, Re, U, and Np, respectively. (b) Experimental data and visually fitted curves of tracer diffusion in saturated granite samples. Simulations of 0.5 and 2 times the fitted apparent diffusivity for Np are also presented to show the sensitivity.

water, heat, and solute movement in one-dimensional, variably saturated media. The HYDRUS program numerically solves the Richards' equation for variably saturated water flow and convection–dispersion-type equations for solute transport of up to ten independent solutes (Simunek et al., 2005). For our saturated diffusion data, only the apparent diffusivity D_a was changed to achieve a good fitting visually; other hydraulic parameters such as porosity, permeability and van Genuchten parameters were obtained from using HYDRUS to inverse fit independent water imbibition tests. The apparent diffusivity (D_a) is related to the effective diffusion coefficient D_e of a sorbing solute as follows:

$$D_a = D_e/R \tag{1}$$

where R is the dimensionless retardation factor that accounts for the interaction of the solute with the porous medium. For a linear sorption isotherm and fast sorption (compared to diffusion)

$$R = 1 + (K_d \times \rho_b)/\theta \tag{2}$$

and K_d is the equilibrium distribution coefficient, ρ_b and are bulk density and porosity, respectively. The effective diffusion coefficient is defined as (Hu and Wang, 2003)

$$D_e = \theta \times \delta \times D_0/\tau \tag{3}$$

with τ (tortuosity, >1) and δ (constrictivity factor, $\leqslant$1; only important in narrow pores) related to the geometry of the porous media, and D_0 the aqueous molecular diffusion coefficient of the diffusant.

Calculated apparent diffusivities are 1.7×10^{-13} m^2/s for nickel and ^{235}U, 8.3×10^{-13} m^2/s for caesium and ^{237}Np, and 8.3×10^{-11} m^2/s for ReO_4^-. Comparing the calculated diffusion profiles with the experimental data in Fig. 5b they show quite reasonable (note the semi-log scale of the figure) fitting for tracers other than ReO_4^-. The poor fitting of ReO_4^- might be related to the fact that the tracer front has reached the other end of the sample. In coarse-grained granite with micro-fractures, diffusion probably occurs in more than one pathway; a multiple-rate diffusion model would have described the data better. However, the apparent diffusivity measured in this preliminary study is quite comparable to those obtained with a through-diffusion method on similar granite samples, with a diffusion coefficient of 8.3×10^{-11} m^2/s for tritium (non-sorbing as ReO_4^-) and 4.3×10^{-14} m^2/s for sorbing caesium.[3]

[3] Havlova, 2007, Nuclear Research Institute, Czech Republic, personal communication.

Table 2
Comparison of measured and predicted diffusion distance

Element	Apparent diffusivity (m^2/s)	Diffusion time (month)	Relative concentration	Diffusion distance (mm)	
				Measured	Predicted
Co; Ni	1.7×10^{-13}	2	0.005	3	3.7
Cs	8.3×10^{-13}	36	0.001	43	41
U	1.7×10^{-13}	2	0.05	4.5	2.6
Np	8.3×10^{-13}	2	0.05	4.5	6.0

3.4. Prediction of in situ diffusion in field dipole test

Based on the derived apparent diffusivities (D_a), we can compare the predicted diffusion distances with those measured from the field dipole test. For a semi-infinite system in which the concentration profile does not reach the end of the sample, the analytical solution to the transient diffusion equation (Fick's second law) is as follows (Crank, 1975; Flury and Gimmi, 2002):

$$\frac{C}{C_0} = \frac{1}{2}\mathrm{erfc}\frac{x}{2\sqrt{D_a \times t}} \quad (4)$$

where C ($M\,L^{-3}$) is the observed concentration at location x based on an initial concentration C_0 ($M\,L^{-3}$), C/C_0 is the relative concentration, x (L) is the diffusion distance, and t (T) is the diffusion time. Using collimated γ-spectrometry with the spatial resolution of several millimetres, Möri et al. (2006) reported maximum ^{137}Cs diffusion into the rock matrix adjacent to a water-conducting fracture to a depth of 45 mm within 3 years and for ^{60}Co to about 3 mm in 2 months. In this study, we obtain a diffusion distance of about 4.5 mm for both uranium and neptunium in the granite matrix near the fracture in 2 months (Fig. 2).

Table 2 presents the comparison of the measured diffusion distance in the field dipole test for four tracers with the predicted distance using the analytical solution of Eq. (4) and laboratory-derived diffusion coefficients. Given the limited data, it is encouraging that comparison shows the numbers to be fairly similar. More data collection and analysis of the spatial distribution of radionuclides in the fracture interface zones that encompass a variety of structural and mineralogical features is currently underway.

4. Summary and conclusions

Fractured granite samples from an *in situ* dipole tracer test at the GTS were analysed to study diffusion profiles of injected radionuclides from a water-conducting feature into the adjacent rock. Micro-scale mapping with LA-ICP-MS showed the presence of long-lived ^{234}U, ^{235}U, and ^{237}Np in flow channels as well as in the adjacent rock. Retardation within the flow field was ascertained on the fracture filling material as well as along the mylonitic sections of the wall rock material, reflecting the increased sorption capacity of the mylonite compared to the rock matrix and the high surface area of the fine grained and highly porous fault gouge material. The maximum penetration depth detected with this technique for ^{237}Np in the granite matrix was up to 10 mm over the 60-day field experiment time scale, illustrating the importance of matrix diffusion in retarding radionuclide transport in water-conducting features.

Diffusion profiles measured in the mylonite on one side of the water-conducting feature and in granitic matrix on the other show that actinides did not penetrate the mylonite as much as the granite matrix. These observations are in good agreement with the physical and chemical characteristics of these rocks; the low porosity and the increased sorption capacity of the mylonites reduce the effective diffusivity in this rock type. On the other hand we also found proof in this study for the potential of structural control on the diffusion paths. In the rock matrix diffusion follows grain boundary pores that form an interconnected pore network with randomly oriented pores. This pore network is clearly less disturbed than the narrow and shear zone parallel oriented pore spaces in the mylonite. Thus tortuosity and constrictivity in the matrix are reduced and diffusion in these rocks is enhanced.

The application of micro-scale LA-ICP-MS technique allowed us to perform short term diffusion experiments with Grimsel granite matrix samples in order to derive apparent diffusion coefficients for the radionuclides present in the water-conducting feature. The measured *in situ* diffusion penetration depth of U and Np could be successfully reproduced as well as ^{137}Cs and ^{60}Co diffusion profiles measured with γ-spectrometry on rock samples from the same water-conducting feature in an earlier study of Möri et al. (2006).

This complementary field, laboratory and modelling study clearly shows the influence of structural and mineralogical alteration on radionuclide transport and the benefit of micro-scale and feature-based LA-ICP-MS to study the role of matrix diffusion of radionuclides in fractured granite.

Acknowledgments

This work was primarily supported by the following partners of the Long Term Diffusion (LTD) project for Phase VI of the GTS: Japan Atomic Energy Agency (JAEA) and National Institute of Advanced Industrial Science and Technology (AIST) of Japan, Radiation and Nuclear Safety Authority (STUK) and University of Helsinki in Finland, Nuclear Research Institute of Czech Republic and NAGRA of Switzerland. Thomas Pettke and Martin Mazurek from the Institute of Geological Sciences of the University of Bern are greatly acknowledged for constructive comments. Financial support from the United States Department of Energy (DOE), Office of Civilian Radioactive Waste Management (OCRWM), and the Office of Chief Scientist (OCS) is also acknowledged. The views, opinions, findings, and conclusions or recommendations expressed herein do not necessarily state or reflect those of the DOE/OCRWM/OCS. The work of the first author was performed under the auspices of the U.S. Department of Energy by Lawrence Livermore National Laboratory under DE-AC52-07NA27344.

References

Abelin, H., Birgersson, L., Moreno, L., Widen, H., Agren, T., Neretnieks, I., 1991. A large-scale flow and tracer experiment in granite. 2. Results and interpretation. Water Resour. Res. 27, 3119–3135.

Alexander, W.R., Bradbury, M.H., McKinley, I.G., Heer, W., Eikenberg, J., Frick, U., 1992. The current status of the radionuclide migration experiment at the Grimsel underground rock laboratory. Sci. Basis Nucl. Waste Manage. XV, 721–728.

Bossart, P., Mazurek, M., 1991. Grimsel test site – structural geology and water flow paths in the migration shear zone. Nagra Technical Report NTB 91-12. Nagra, Wettingen, Switzerland.

Crank, J., 1975. The Mathematics of Diffusion, second ed. Oxford University Press Inc., New York.

Dai, Z., Wolfsberg, A., Lu, Z., Reimus, P., 2007. Upscaling matrix diffusion coefficients for heterogeneous fractured rocks. Geophys. Res. Lett. 34, L07408. doi:10.1029/2007GL02933.

Eikenberg, J., Ruethi, M., Alexander, W.R., Frieg, B., Fierz T., 1998. The excavation project in the Grimsel Test Site – in situ high resolution gamma and alpha spectrometry of Co-60, Se-75, Sn-113, Eu-152 and Np-237/Pa-233. In: MRS Symposium Proceedings, vol. 506, pp. 655–662.

Flury, M., Gimmi, T.F., 2002. Solute diffusion. in methods of soil analysis. Part 4 – physical methods. In: Dane J.H., Topp G.C. (Eds.), Soil Sci. Soc. Am., Madison, WI, pp. 1323–1351.

Frieg, B., Alexander, W.R., Dollinger, H., Bühler, C., Haag, P., Möri, A., Ota, K., 1998. In situ impregnation for investigating radionuclide retardation in fractured repository host rocks. J. Contam. Hydrol. 35, 115–130.

Grisak, G.E., Pickens, J.F., 1980. Solute transport through fractured media. Part I: the effect of matrix diffusion. Water Resour. Res. 16, 719–730.

Hadermann, J., Heer, W., 1996. The Grimsel (Switzerland) migration experiment: Integrating field experiments, laboratory investigations and modelling. J. Contam. Hydrol. 21, 87–100.

Hu, Q., Wang, J.S.Y., 2003. Aqueous-phase diffusion in unsaturated geologic media: a review. Crit. Rev. Environ. Sci. Technol. 33, 275–297.

Hu, Q., Salve, R., Stringfellow, W.T., Wang, J.S.Y., 2001. Field tracer transport tests in unsaturated fractured tuffs. J. Contam. Hydrol. 51, 1–12.

Hu, Q., Kneafsey, T.J., Wang, J.S.Y., Tomutsa, L., Roberts, J.J., 2004. Characterizing unsaturated diffusion in porous tuff gravels. Vadose Zone J. 3, 1425–1438.

Lide, D.R. (Ed.), 2000. CRC Handbook of Chemistry and Physics. CRC Press, Boca Raton, Florida.

Maloszewski, P., Zuber, A., 1993. Tracer experiments in fractured rocks – matrix diffusion and the validity of models. Water Resour. Res. 29 (8), 2723–2735.

Meigs, L.C., Beauheim, R.L., 2001. Tracer tests in a fractured dolomite. 1. Experimental design and observed tracer recoveries. Water Resour. Res. 37, 1113–1128.

Möri, A., Schild, M., Siegesmund, S., Vollbrecht, A., Adler, M., Mazurek, M., Ota, K., Haag, P., Ando, T., Alexander, W.R., 2003. The Nagra-JNC in situ study of safety relevant radionuclide retardation in fractured crystalline rock IV: the in situ study of matrix porosity in the vicinity of a water-conducting fracture. Nagra Technical Report NTB 00-08, Nagra, Wettingen, Switzerland.

Möri, A., Biggin, C., Mäder, U., Eikenberg, J., Rüthi, M., 2006. Novel application of β/γ autoradiography and collimated γ-spectrometry to study in situ radionuclide migration paths in fractured rock. Phys. Chem. Earth, Parts A/B/C 31, 511–516.

Neretnieks, I., 1980. Diffusion in the rock matrix: an important factor in radionuclide migration? J. Geophys. Res. 85, 4379–4397.

Nordstrom, D.K., Olsson, T., Carlsson, L., Fritz, P., 1989. Introduction to the hydrogeochemical investigations within the international stripa project. Geochim. Cosmochim. Acta 53 (8), 1717–1726.

Novakowski, K.S., Lapcevic, P.A., 1994. Field measurement of radial solute transport in fractured rock. Water Resour. Res 30, 37–44.

Russo, R.E., Mao, X.L., Borisov, O.V., Liu, H.C., 2000. Laser ablation in atomic spectroscopy. Encyclopedia of Analytical Chemistry: Instrumentation and Applications. John Wiley & Sons Ltd., Chichester.

Russo, R.E., Mao, X.L., Liu, H.C., Gonzalez, J., Mao, S.S., 2002. Laser ablation in analytical chemistry – a review. Talanta 57, 425–451.

Salve, R., Liu, H.H., Cook, P., Czarnomski, A., Hu, Q., Hudson, D., 2004. Unsaturated flow and transport through a fault embedded in fractured welded tuff. Water Resour. Res. 40, W04210. doi:10.1029/2003WR00257.

Sardini, P., Siitari-Kauppi, M., Beaufort, D., Hellmuth, K.H., 2006. On the connected porosity of mineral aggregates in crystalline rocks. Am. Mineral. 91, 1069–1080.

Simunek, J., van Genuchten, M.Th., Sejna, M., 2005. The HYDRUS-1D Software Package for Simulating the Movement of Water, Heat, and Multiple Solutes in Variably Saturated Media, Version 3.0, HYDRUS Software Series 1, Department of Environmental Sciences, University of California Riverside, Riverside, CA, USA, 270 p.

Smith, P.A., Alexander, W.R., Kickmaier, W., Ota, K., Frieg, B., McKinley, I.G., 2001. Development and testing of radionuclide transport models for fractured rock: examples from the Nagra/JNC radionuclide migration programme in the Grimsel test site, Switzerland. J. Contam. Hydrol. 47, 335–348.

Sylvester, P.J., 2005. Laser ablation ICP-MS developments and trends for 2003. Geostandard Geoanal. Res. 29, 41–52.

Zhou, Q.L., Liu, H.H., Bodvarsson, G.S., Molz, F.J., 2006. Evidence of multi-process matrix diffusion in a single fracture from a field tracer test. Transp. Porous Media 63, 473–487.